NANO LETTERS

Letter

pubs.acs.org/NanoLett

Evidence for Structural Phase Transitions Induced by the Triple Phase Line Shift in Self-Catalyzed GaAs Nanowires

Xuezhe Yu,[†] Hailong Wang,[†] Jun Lu,[†] Jianhua Zhao,*[,†] Jennifer Misuraca,[‡] Peng Xiong,[‡] and Stephan von Molnár[‡]

[†]State Key Laboratory of Superlattices and Microstructures, Institute of Semiconductors, Chinese Academy of Sciences, P.O. Box 912, Beijing 100083, China

[‡]Department of Physics, Florida State University, Tallahassee, Florida 32306, United States

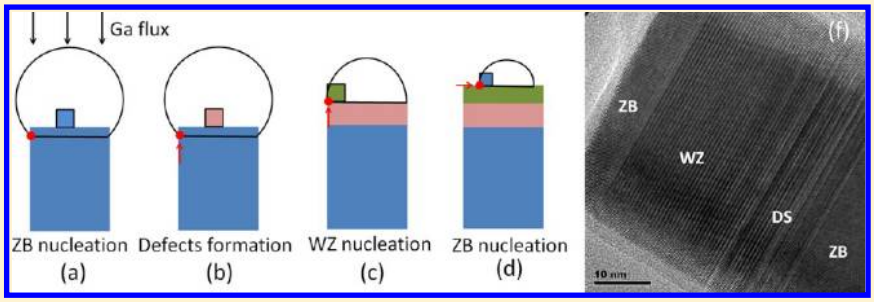

ABSTRACT: Self-catalyzed growth of GaAs nanowires are widely ascribed to the vapor−liquid−solid (VLS) mechanism due to the presence of Ga particles at the nanowire tips. Here we report synthesis of self-catalyzed GaAs nanowires by molecular-beam epitaxy covering a large growth parameter space. By carefully controlling the Ga flux and its ratio with the As flux, GaAs nanowires without Ga particles and exhibiting a flat growth front are produced. Using scanning electron microscopy and high-resolution transmission electron microscopy, we compare the growth rate and structure, especially near the growth front, of the nanowires with and without Ga droplets. We find that regardless of whether Ga droplets are present on top, the nanowires have a short wurtzite section following the zinc-blende bulk structure. The nanowires without Ga droplets are terminated by a thin zinc-blende cap, while the nanowires with Ga droplets do not have such a cap. The bulk zinc-blende phase is attributed to the Ga droplet wetting the sidewall during growth, pinning the triple phase line on the sidewall. The zinc-blend/wurtzite/(zinc-blende) phase transitions at the end of growth are fully consistent with the triple phase line shifting up to the growth front due to the progressive consumption of the Ga in the droplet by crystallization with As. The results imply an identical VLS growth mechanism for both types of GaAs NWs, and their intricate structures provide detailed comparison with and specific experimental verification of the recently proposed growth mechanism for self-catalyzed III−V semiconductor nanowires (*Phy. Rev. Lett.* **2011**, *106*, 125505). Using this mechanism as a guideline, we successfully demonstrated controllable fabrication of two distinct types of axial superlattice GaAs NWs consisting of zinc-blende/defect-section and wurtzite/defect-section units.

KEYWORDS: *Molecular-beam epitaxy, semiconductor nanowires, nanowire growth kinetics, structural transition of nanowires*

Self-assembled semiconductor nanowires (NWs) have attracted extensive interest in the past decade due to their potential as building blocks for future semiconductor electronic, photonic, and sensing devices with multifunctional capabilities and higher performance.[1−3] III−V semiconductor NWs are an important class of the vast semiconductor NW family because of the extensive applications of their bulk counterparts in microelectronics and photonics. So far, most of the III−V NWs investigated are produced via a particle-assisted growth mechanism, whose notable characteristic is the existence of nanoparticles on top of the resulting NWs.[4] These particles are in either a liquid or solid state during growth. In the former case, the growth mechanism is the so-called vapor−liquid−solid (VLS) mechanism[5] and for the latter, it is referred to as the vapor−solid−solid mechanism.[6] In principle, for particle-assisted growth mechanisms the primary function of the particle is to collect source material from the vapor phase, which results in a supersaturated state of source material in the particle and facilitates nucleation and precipitation of the source material at the interface between the particle and the solid NWs.[7] In order to generate such particles, catalytic material is normally needed to form an alloy with the source material whose eutectic temperature is below the melting point of the solid phase of the NWs. At present, there are two methods to form particles which can function as catalysts. One is by using foreign material, among which gold is the most common. The other one utilizes the low melting point of one of the source materials (typically a metal) to create liquid droplets and thus is often called self-catalyzed growth. In some of the prominent examples, Ga droplets for GaAs NWs and In droplets for InAs and InP NWs are created. Because of

Received: September 6, 2012

   dx.doi.org/10.1021/nl303323t | *Nano Lett.* XXXX, XXX, XXX−XXX

the critical role of these droplets in the NW growth, many investigations have been focused on states and composition of these particles.[6,8] In contrast to NWs grown by using foreign catalysts for which the catalyst particles are observable during and after growth,[8] droplets for self-catalyzed NWs, such as InAs, sometimes are absent in the end products.[9−11] Consequently, there has been much debate about whether such NWs are grown via a VLS or non-VLS mechanism.[4,9−11] Furthermore, it has been pointed out that the shape and size of the droplet and the resulting mechanism of nucleation in the droplet significantly influences the structural phase of the NWs.[12−15] Therefore, a clear understanding of the behavior of the droplets could lead to deeper insight of the growth front at the droplet/NW interface, which is closely related to the growth kinetics as well as the structural and physical properties of the NWs. An important recent development is a theoretical model by Krogstrup et al.[15] describing a growth mechanism with which the structure of the self-catalyzed III−V NWs is controlled by the shape, relative volume, and wetting condition of the Ga droplet. While the model is able to account for various structural details in a host of GaAs NWs, a systematic comparison with experiments over the entire range of Ga droplet shape and volume is lacking.

In this Letter, we report on the growth and structural analysis of self-catalyzed GaAs NWs by molecular-beam epitaxy (MBE). We choose GaAs NWs because, unlike InAs NWs, there have been many reports of self-catalyzed growth of GaAs NWs which is ascribed to a VLS mechanism due to the presence of Ga droplets.[14,16−19] Here, by tuning the growth parameters carefully, we reveal a small parameter space in which GaAs NWs without any droplets are produced. By comparing the structures of the NWs with and without Ga droplets, we deduce a common VLS growth mechanism for both types of NWs controlled by the position of the triple phase line (TPL). The shift of the TPL at the end of the growth (due to the progressive consumption of the Ga in the droplets) from the sidewall to the top edge of the growth front, and toward the center of the growth front in the case of NWs without Ga droplets, offers a straightforward and consistent explanation for the NW structures, particularly the complex phase transitions at the NW ends. The results offer the experimental basis for a systematic, thorough, and rigorous comparison with the recently proposed growth model for self-catalyzed III−V semiconductor nanowires.[15] Moreover, as a precise test of the applicability of this mechanism, we successfully fabricated two distinct types of homosuperlattices of GaAs NWs consisting of zinc-blende/defect-section and wurtzite/defect-section units, demonstrating a high degree of structural control for the synthesis process.

The GaAs NWs were grown in a solid source MBE system (V80 MARKI). Commercial *n*-type silicon (111) wafers were used as the substrates. Before moving the silicon substrates into the MBE system, they were dipped into buffered HF aqueous solution (5%) for 2 s to remove surface contamination, leaving a thin layer of dioxide with pinholes.[4,16] Next, they were rinsed with deionized H_2O and dried by a nitrogen gas stream. After the samples were loaded into the growth chamber of the MBE system, the substrate temperature was increased to 680 °C and the substrate was annealed for 5 min for further elimination of contaminants on the surface, after which the temperature was lowered to the appropriate growth temperature. For all samples, we started the growth by opening the Ga shutter 10 s prior to that of As. We expected that the procedure above would favor the formation of Ga droplets, which are essential for GaAs NWs growth via a VLS mechanism.

In total, four series of samples were grown. Series A consists of samples grown with various Ga fluxes ranging from 0.2 to 2.2 Å/s. The fluxes are given as equivalent nominal growth rates of planar GaAs films which are calibrated by reflection high-energy electron diffraction (RHEED) oscillations at normal growth conditions (V/III = 15) for GaAs on a GaAs (001) substrate. Series B consists of samples grown with different As fluxes, whose V/III = 3.03, 3.84, 6.72, 10.16, and 16.82 respectively, each of which is the ratio of their beam equivalent pressure, while the Ga flux is fixed at 2.2 Å/s. Samples of both series were grown for a duration of 40 min and at a temperature of 640 °C. We then synthesized series C and D for direct comparison, where we adopted a slightly larger As flux than that of series A, while the Ga flux is fixed at 0.5 Å/s (1.0 Å/s) for series C (series D). Growth time varied from 5 to 80 min. For all samples, the substrate temperature was fixed at 640 °C. At the end of the growth, the Ga and As shutters were closed simultaneously.

For postgrowth measurements, we used scanning electron microscopy (SEM) from which information about the surface density and the growth rate of the ensembles of NWs was obtained, and transmission electron microscopy (TEM) for an atomic level examination of the morphology and crystal structure. For all the high-resolution transmission electron microscopy (HRTEM) measurements, the electron beam was aligned along the [1−10] direction.

GaAs NWs were obtained for all growth conditions of series A and B, covering a vast growth window. As shown in Figure 1,

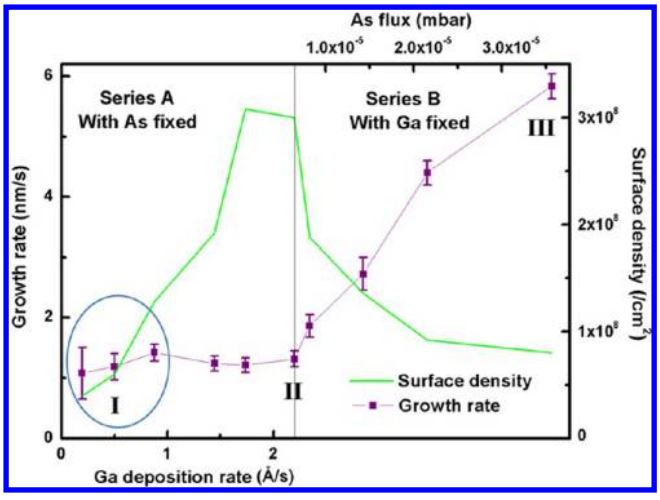

Figure 1. Surface density and growth rate of GaAs NWs as a function of Ga flux (left panel) and As flux (right panel). Series A has As flux fixed at 6.0×10^{-6} mbar and series B has Ga flux fixed at 2.2 Å/s. The point II has both of these values. The blue ellipse is added to show the range where NWs uniform in diameters and without droplets are grown. I, II, and III are samples that we used in HRTEM measurements discussed below.

the surface density varies with changing Ga and As fluxes. This can be explained with the expectation that a larger Ga flux will create more droplets, while in contrast, Ga droplets are difficult to generate in heavy As flux. The growth rate of NWs is dependent on As flux rather than Ga flux indicating that the local environment for nucleation is a Ga-rich one. This observation is consistent with the scheme of a VLS mechanism

dx.doi.org/10.1021/nl303323t | *Nano Lett.* XXXX, XXX, XXX−XXX

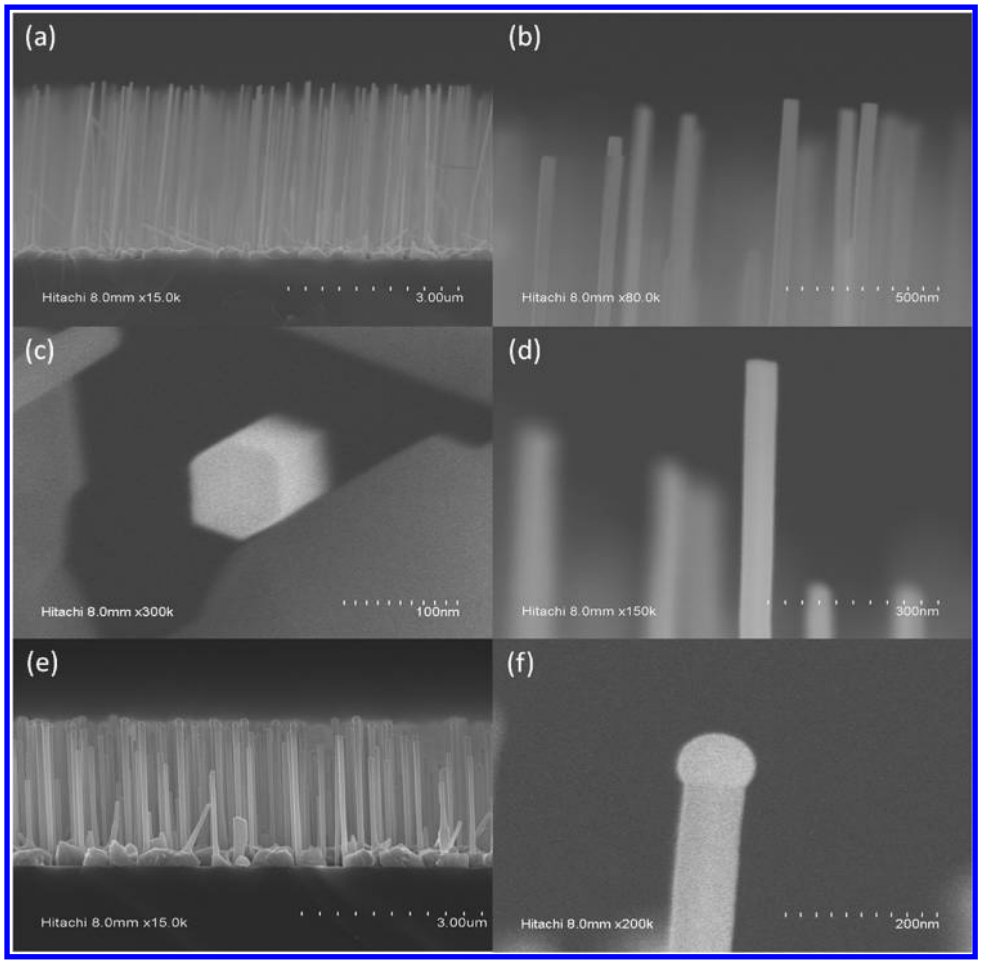

Figure 2. Side-view SEM images of GaAs NWs from series A: (a–d) NWs without droplets for a sample with a Ga flux of 0.88 Å/s; (e,f) NWs with droplets with a Ga flux of 2.2 Å/s. All other growth parameters were fixed.

where the vapor phase of As is absorbed by Ga droplets, and GaAs is precipitated to yield the NW body. It is also in agreement with the reports that indicate that larger As flux results in longer self-catalyzed GaAs NWs.[16]

We emphasize here the observation of the *absence* of Ga droplets in the NWs for a certain growth window, and the resulting structural phase transitions near the end of the NWs. We observe that more NWs lost their droplets when Ga flux became smaller for our choice of As flux; and when it is less than 0.88 Å/s nearly all NWs have a flat growth front (Figures 1 and 2), similar to the case of InAs NWs.[9−11] Although the absence of Ga droplets and the flat growth front do not necessarily require a new growth mechanism for these NWs, the fact that self-catalyzed GaAs NWs both with and without Ga droplets can be synthesized offers us a unique opportunity of elucidating new insights into the growth mechanism of self-catalyzed NWs.

We first compared the lengths of the NWs under two carefully chosen conditions for different growth durations with the expectation that different growth mechanisms would result in different growth rates. For direct and unambiguous comparison, two new series of NWs were synthesized: Series C (D) corresponds to NWs without (with) Ga droplets and the results are given in Figure 3a. Figure 3 panels b and c and panels d and e show representative SEM images for series C and D, respectively, with the same growth time of 80 min. Contrary to expectation, the growth rates of series C and D are almost identical, implying a surprising VLS growth mechanism even for NWs without droplets (series C), just as for the NWs with droplets in series D. The absence of Ga droplets in series C can be interpreted as the complete crystallization of the Ga with As into the NW body during the cool-down process, even though it takes less than 20 s to decrease from 640 °C (growth temperature) to 560 °C, and below 560 °C no axial growth is observed. This assertion is supported by further HRTEM measurements on several samples (Figure 4). Samples I and III have a crystallized top facet without a droplet and sample II has an amorphous Ga droplet atop the NW. Moreover, we observe that sample III has a tapered top, while for samples I and II no obvious decrease in diameter is found. Such variation in diameter usually happens because of rapid crystallization of the Ga droplet in As ambient after the Ga source is closed.[20] For sample III, this sudden decrease of source material was reflected in the diameter variation of the NW because of the high crystallization rate, while for samples I and II, owing to the relatively low growth rate, the Ga droplets had sufficient time to relax and nearly no change in diameter is observed. We therefore conclude that a droplet is present on top of the NW during growth even for samples I and III, but disappears only during the cool-down process.

Another notable observation is a section of wurtzite (WZ) phase found near the top in each of the three samples with different growth conditions as revealed by HRTEM. Particularly, for sample III this section of WZ phase is where the

dx.doi.org/10.1021/nl303323t | *Nano Lett.* XXXX, XXX, XXX–XXX

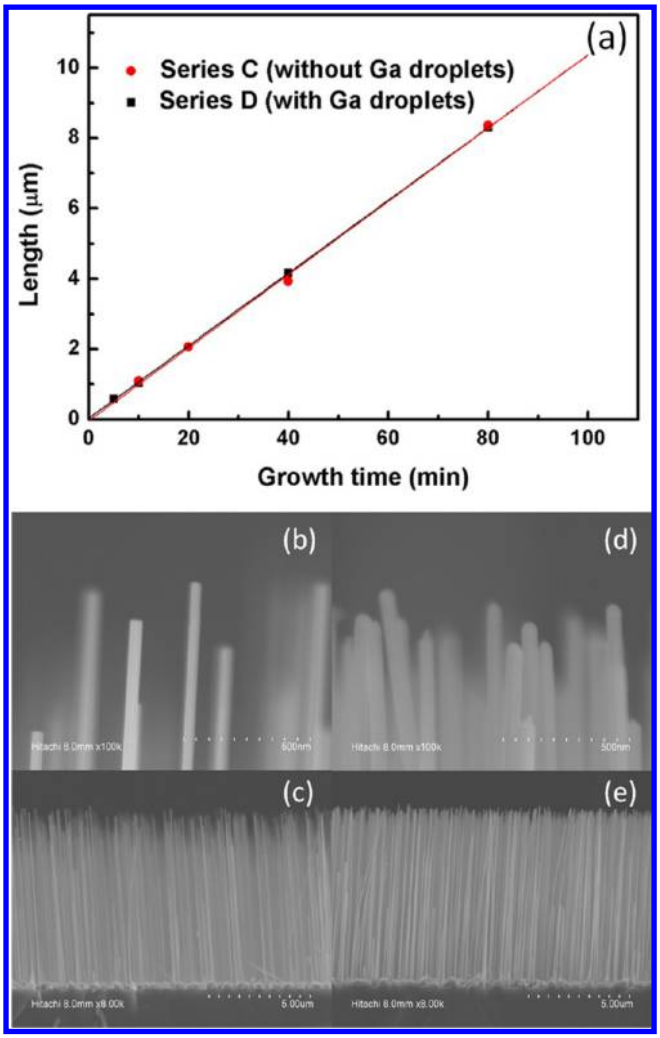

Figure 3. Comparison of the growth rates of GaAs NWs without Ga droplets (series C) and those with Ga droplets (series D)(a). SEM images for GaAs NWs without droplets ((b), (c)) and with droplets ((d), (e)) grown for 80 min.

diameter decrease occurs. These observations lead us to the conclusion that the emergence of the WZ phase is a direct consequence of the ceasing of the supply of the Ga source material. Furthermore, for samples I and III in which there is no Ga droplet at the top, there exists a short zinc-blende (ZB) cap above the WZ section; in contrast, for sample II in which an amorphous droplet takes up the top position, there is no such ZB section. TEM and HRTEM measurements were also implemented on the GaAs NW body and several typical images are given in Figure 5. Figure 5a shows a series of TEM images of a NW over its entire length. HRTEM verifies the ZB structure of the bulk (Figure 5b) and WZ structure of a section near the tip (Figure 5c) of the NW. Importantly, every single planar defect in the NW was examined by HRTEM to determine the crystal structure intentionally and was confirmed to be a twin-plane defect (e.g., Figure 5d). Hence the GaAs NW is of a pure ZB structure without any WZ phase except at the tip.

Next, we describe a scheme for the self-catalyzed GaAs NW growth that consistently accounts for all these observations, especially the complex structures and transitions of phases near the top of the NWs. The mechanism is based on the shift of the TPL position and nucleation sites along the NW during the entire growth process, which is illustrated in Figure 6. A full three-dimensional model of the scheme is described in detail in ref 15. Here we utilized a simplified two-dimensional version based on 2D nucleation theory.[12,14] The shift of the TPL position is due to the evolution of the shape and volume of the Ga droplet near the end of growth. It has been widely accepted that TPL nucleation favors the WZ phase growth in the standard VLS mechanism where the droplet only wets the top facet of the NW (as in Figure 6c).[12] However, pure ZB structure in our GaAs NWs as well as those in the previous work,[14,17,18] indicates the breakdown of the TPL nucleation. As discussed in ref 17, due to the low surface energy of the Ga droplet the TPL nucleation is not stable for Ga droplet-assisted GaAs NWs. Moreover, ref 14 reported specifically treated GaAs NWs grown by a novel VLS mechanism, where the sidewall of the NWs was wetted by Ga droplets due to the low liquid–vapor surface energy of Ga droplets, so that WZ nucleation was prohibited. Therefore, our observation supports the scenario of suppression of TPL nucleation by sidewall wetting, but we believe this is a common growth mechanism for a vast growth window rather than a case of subtle energetic difference. Figure 6a depicts the growth of the bulk of the GaAs NW, where the growth is in a stable state. As mentioned above, the resulting ZB structure is due to the TPL being on the sidewall instead of on top of the NW. When the Ga flux is stopped (Figure 6b), the amount of Ga in the droplet begins to decrease. The TPL retreats along the sidewall of the NW, generating a transition layer consisting of twin plane and stacking fault defects, until it reaches the top of the NW (Figure 6c). Consumption of the remaining Ga in the droplet generates a WZ phase due to the TPL nucleation, as in the standard VLS mechanism (Figure 6c).[12] Between the previous two processes, an observable variation in diameter would happen depending on the size of the Ga droplet and the axial growth rate of the GaAs NW. When the droplet becomes small to some degree it will withdraw again along the NWs top facet due to the decrease of the contact angle, leading to a ZB phase because of the unconstrained nucleation on the flat surface as well as the possible breakdown of the condition for TPL nucleation (Figure 6d).[12,15] This is verified by the HRTEM images for samples I and III in the case of full crystallization (Figures 4 and 6f). Therefore, the apparently complex ZB/WZ/ZB phase transitions can be straightforwardly explained by the process described here. It is worthwhile to mention that such a ZB/WZ/ZB structure was also reported in the ref 19. There, the ZB→WZ transition was observed to happen in the middle of the nanowire, which is difficult to attribute to the shift of the TPL, especially since stacking faults and the ZB→WZ transition can be caused by other mechanisms and factors.[21−23] In our case, we never observed any WZ phase in the body of the self-catalyzed GaAs NWs grown in the vast parameter space (Figure 5), which can be explained by the long diffusion length of Ga atoms on the silicon dioxide surface.[24] The difference may be due to different states of the substrate surface: wafers with native silicon dioxide were used in ref 19 while in the present work the surface was carefully prepared with an elaborate treatment. The structural evolution at the end of the NWs is also consistent with a rough calculation based in Figure 6f that shows that the height of the pure Ga droplet is around 25 nm in the Figure 6c state. Given that the diameter of the NW is 52 nm, the droplet is nearly hemispheric. If the As dissolved in the Ga droplet is taken into account, the contact angle would be

dx.doi.org/10.1021/nl303323t | *Nano Lett.* XXXX, XXX, XXX−XXX

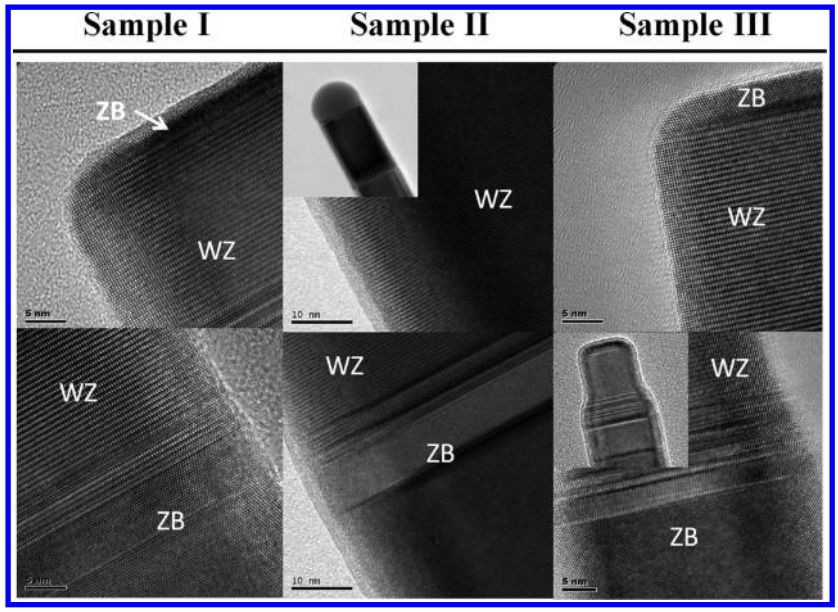

Figure 4. HRTEM images for samples I, II and III. The growth conditions for the three samples are indicated in Figure 1. The top panels are images of the sections at the very end of the NWs, and the bottom panels are images of the section just below the wurtzite phase. The top inset shows the amorphous droplet of sample II. The bottom inset shows the reduced diameter of the wurtzite section of sample III.

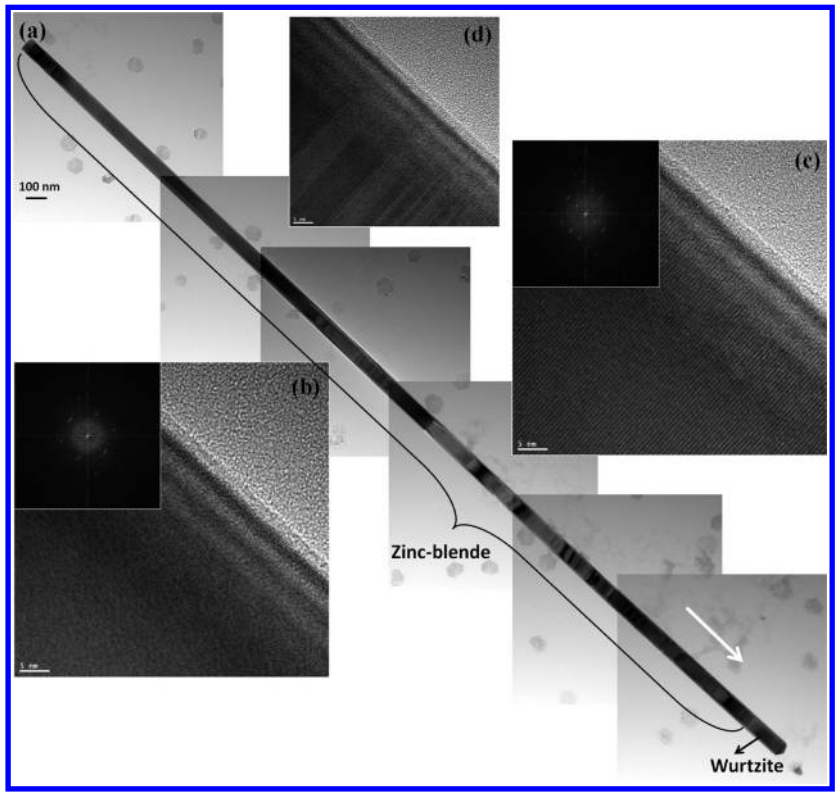

Figure 5. (a) TEM images of a GaAs NW over its entire length. The white arrow indicates the growth direction. (b) HRTEM image of a section from bulk, showing zinc-blende phase. (c) HRTEM image of the wurtzite section at the NW tip. (d) HRTEM image of a section just below the wurtzite phase, showing twin-plane defects. The insets in (b) and (c) are the fast Fourier transform (FFT) of (b) and (c), respectively.

even larger than 90°, as exemplified in Figure 2f, which is consistent with previous reports.[14,17]

Finally, as a stringent test of the predictive power of the TPL shift model, we designed and fabricated two types of homosuperlattice GaAs NWs. They are defect-free ZB/defect−section (DS) and defect-free WZ/DS superlattice structures, as shown in Figure 7a,b, respectively. The TPL shift is controlled mainly through the growth rate of NWs. By choosing appropriate As flux and opening and closing the Ga source shutter, we expect to obtain various combination of WZ, ZB, and DS sections in a single GaAs NW, whose length is determined by the duration of opening or closing the Ga shutter. Depending on the Ga droplet volume, even a fairly long section of WZ phase in principle could be achieved in a

dx.doi.org/10.1021/nl303323t | Nano Lett. XXXX, XXX, XXX−XXX

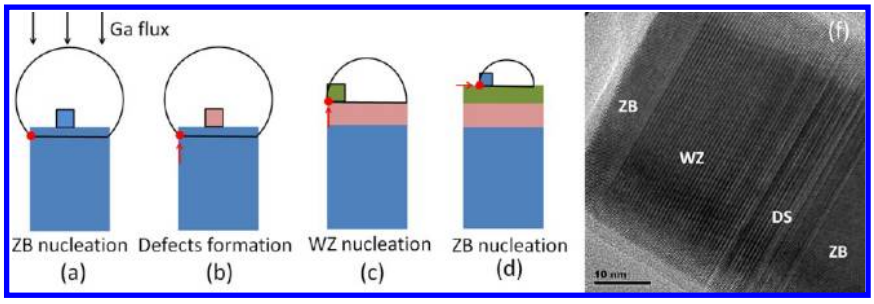

Figure 6. Illustrations of the effect of the droplet on the crystal structure of the GaAs NW. The red dots and arrows indicate the positions and moving directions respectively of the TPL. Blue and green indicate zinc-blende and wurtzite phases respectively. (a) Droplet wets sidewall leading to center nucleation. (b) TPL shifts along the sidewall. (c) Standard TPL nucleation leads to wurtztite phase. (d) Droplet retreats along the top facet. (f) An HRTEM image illustrates zinc-blende/wurtzite/zinc-blende transition.

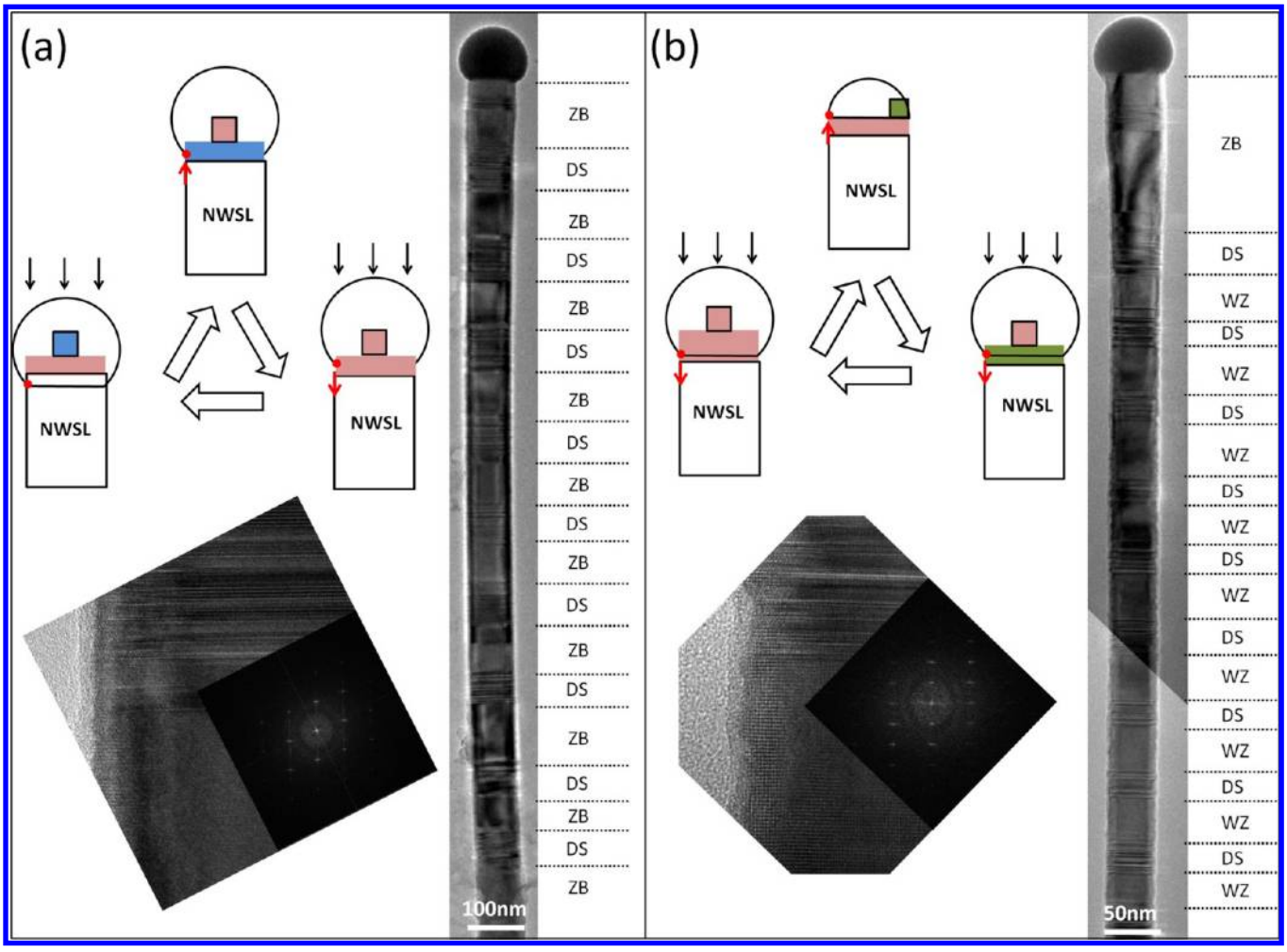

Figure 7. The TEM image and schematic structure of (a) zinc-blende/defect-section superlattice and (b) wurtzite/defect-section superlattice GaAs NWs. A typical interface image (including the FFT image from defect-free section) and illustration of the growth mechanism are also given for each.

ZB GaAs NW. Here, we present TEM images of two representative NWs in Figure 7. In a single GaAs NW, ZB (Figure 7a) or WZ sections (Figure 7b) are separated by the defect-sections. The most notable characteristic of our strategy for fabricating the homoheterostructrual NWs is that the morphological and structural properties of each section can be fully controlled. When growing these superlattice NWs, we ended the growth by closing the As shutter, so these NWs were terminated with a ZB section. To the best of our knowledge, such superlattice NWs have not been reported before, probably because defects, both twin plane and stacking fault, are as difficult to control as the pure ZB or WZ phase.

In summary, through fine control of the growth conditions, we have controllably produced self-catalyzed GaAs NWs with and without Ga droplets. SEM and HRTEM images reveal the same bulk structure but subtle and consistent differences at the growth front for the two types of NWs. Most notably, the NWs without Ga droplets exhibit a ZB/WZ/ZB phase transition at the end. A VLS growth mechanism based on the shift of the TPL from the sidewall to the top of the NW, offers a consistent

dx.doi.org/10.1021/nl303323t | *Nano Lett.* XXXX, XXX, XXX−XXX

account of all the structural features in both types of NWs and the disappearance of the Ga droplets under certain growth conditions. The results can be fully accounted for by the recently proposed growth model for self-catalyzed III−V semiconductor nanowires,[15] thus providing a rigorous and systematic verification of the theory. These insights on the growth mechanism of the self-catalyzed GaAs NWs could provide important and reliable guidelines on the control and optimization of the structural and physical properties of the NWs. The successful synthesis of the two types of preconceived axial superlattice structures in the self-catalyzed GaAs NWs based on the TPL shift mechanism has provided encouraging evidence for the approach.

AUTHOR INFORMATION

Corresponding Author

*E-mail: jhzhao@red.semi.ac.cn.

Notes

The authors declare no competing financial interest.

ACKNOWLEDGMENTS

The authors acknowledge K. K. Meng, S. L. Wang, D. Pan, and S. H. Nie for their assistance in sample preparation. J.H.Z. thanks MOST of China for Grant 2012CB932701 and NSFC for Grants 60836002 and 10920101071. S.v.M. and P.X. acknowledge NSF Materials World Network Grant DMR-0908625.

REFERENCES

(1) Lieber, C. M.; Wang, Z. L. *MRS Bull.* **2007**, *32*, 99.
(2) Yan, R. X.; Gargas, D.; Yang, P. D. *Nat. Photonics* **2009**, *3*, 569.
(3) Patolsky, F.; Lieber, C. M. *Mater. Today* **2005**, *8*, 20.
(4) Mandl, B.; Stangl, J.; Hilner, E.; Zakharov, A. A.; Hillerich, K.; Dey, A. W.; Samuelson, L.; Bauer, G.; Deppert, K.; Mikkelsen, A. *Nano Lett.* **2010**, *10*, 4443.
(5) Wagner, R. S.; Ellis, W. C. *Appl. Phys. Lett.* **1964**, *4*, 89.
(6) Persson, A. I.; Larsson, M. W.; Stenström, S.; Ohlsson, B. J.; Samuelson, L.; Wallenberg, L. R. *Nat. Mater.* **2004**, *3*, 677.
(7) Wacaser, B. A.; Dick, K. A.; Johansson, J.; Borgström, M. T.; Deppert, K.; Samuelson, L. *Adv. Mater.* **2009**, *21*, 153.
(8) Dick, K. A. *Prog. Cryst. Growth Charact. Mater.* **2008**, *54*, 138.
(9) Mandl, B.; Stangl, J.; Mårtensson, T.; Mikkelsen, A.; Eriksson, J.; Karlsson, L. S.; Bauer, G.; Samuelson, L.; Seifert, W. *Nano Lett.* **2006**, *6*, 1817.
(10) Hertenberger, S.; Rudolph, D.; Bolte, S.; Döblinger, M.; Bichler, M.; Spirkoska, D.; Finley, J. J.; Abstreiter, G.; Koblmüller, G. *Appl. Phys. Lett.* **2011**, *98*, 123114.
(11) Dimakis, E.; Lähnemann, J.; Jahn, U.; Breuer, S.; Hilse, M.; Geelhaar, L.; Riechert, H. *Cryst. Growth Des.* **2011**, *11*, 4001.
(12) Glas, F.; Harmand, J. C.; Patriarche, G. *Phy. Rev. Lett.* **2007**, *99*, 146101.
(13) Dubrovskii, V. G.; Sibirev, N. V.; Harmand, J. C.; Glas, F. *Phys. Rev. B* **2008**, *78*, 235301.
(14) Dubrovskii, V. G.; Cirlin, G. E.; Sibirev, N. V.; Jabeen, F.; Harmand, J. C.; Werner, P. *Nano Lett.* **2011**, *11*, 1247.
(15) Krogstrup, P.; Curiotto, S.; Johnson, E.; Aagesen, M.; Nygård, J.; Chatain, D. *Phy. Rev. Lett.* **2011**, *106*, 125505.
(16) Colombo, C.; Spirkoska, D.; Frimmer, M.; Abstreiter, G.; Fontcuberta i Morral, A. *Phys. Rev. B* **2008**, *77*, 155326.
(17) Cirlin, G. E.; Dubrovskii, V. G.; Samsonenko, Y. B.; Bouravleuv, A. D.; Durose, K.; Proskurvakov, Y. Y.; Mendes, B.; Bowen, L.; Kaliteevski, M. A.; Abram, R. A.; Zeze, D. *Phys. Rev. B* **2010**, *82*, 035302.
(18) Krogstrup, P.; Popovitz-Biro, R.; Johnson, E.; Madsen, M. H.; Nygard, J.; Shtrikman, H. *Nano Lett.* **2010**, *10*, 4475.
(19) Plissard, S.; Dick, K. A.; Larrieu, G.; Godey, S.; Addad, A.; Wallart, X.; Caroff, P. *Nanotechnology* **2010**, *21*, 385602.
(20) Plante, M. C.; LaPierre, R. R. *Nanotechnology* **2008**, *19*, 495603.
(21) Johansson, J.; Karlsson, L. S.; Dick, K. A.; Bolinsson, J.; Wacaser, B. A.; Deppert, K.; Samuelson, L. *Cryst. Growth Des.* **2009**, *9*, 765.
(22) Chiaramonte, Thalita.; Tizei, L. H. G.; Ugarte, D.; Cotta, M. A. *Nano Lett.* **2011**, *11*, 1934.
(23) Ikejiri, K.; Kitauchi, Y.; Tomioka, K.; Motohisa, J.; Fukui, T. *Nano Lett.* **2011**, *11*, 4314.
(24) Heiß, M.; Riedlberger, E.; Spirkoska, D.; Bichler, M.; Abstreiter, G.; Fontcuberta I Morral, A. *J. Cryst. Growth* **2008**, *310*, 1049.